Proc. Natl. Acad. Sci. USA
Vol. 84, pp. 7846–7850, November 1987
Biochemistry

Molecular architecture of rabbit skeletal muscle aldolase at 2.7-Å resolution

(fructose 1,6-bisphosphate/protein crystallography/enzymatic mechanism/three-dimensional structure)

J. SYGUSCH*, D. BEAUDRY, AND M. ALLAIRE

Département de Biochimie, Faculté de Médecine, Université de Sherbrooke, Sherbrooke, PQ J1H 5N4, Canada

Communicated by Frederic M. Richards, July 20, 1987 (received for review February 3, 1987)

ABSTRACT **The molecular architecture of the rabbit skeletal muscle aldolase (D-fructose-1,6-bisphosphate D-glyceraldehyde-3-phosphate-lyase, EC 4.1.2.13) tetramer has been determined to 2.7-Å resolution. Solution of the three-dimensional structure of rabbit muscle aldolase utilized phase information from a single isomorphous $Pt(CN)_4^{2-}$ derivative, which was combined with iterative-phase refinement based upon the noncrystallographic 222-fold symmetry exhibited by the tetramer subunits. The electron-density map calculated from the refined phases (m_f = 0.72) was interpreted on the basis of the known amino acid sequence (363 amino acids per subunit). The molecular architecture of the aldolase subunit corresponds to a singly wound β-barrel of the parallel α/β class structures as has been observed in triose phosphate isomerase, pyruvate kinase, phosphogluconate aldolase, as well as others. Close contacts between tetramer subunits are virtually all between regions of hydrophobic residues. Contrary to other β-barrel structures, the known active-site residues are located in the center of the β-barrel and are accessible to substrate from the COOH side of the β-barrel. Biochemical and crystallographic data suggest that the COOH-terminal region of aldolase covers the active-site pocket from the COOH side of the β-barrel and mediates access to the active site. On the basis of sequence studies, active-site residues as well as residues lining the active-site pocket have been totally conserved throughout evolution. By comparison, homology in the COOH-terminal region is minimal. It is suggested that the amino acid sequence of the COOH-terminal region may be, in part, the basis for the variable specific activities aldolases exhibit toward their substrates.**

Aldolase (D-fructose-1,6-bisphosphate D-glyceraldehyde-3-phosphate-lyase, EC 4.1.2.13) is an ubiquitous and abundant glycolytic enzyme that plays a central and pivotal role in glycolysis and fructose metabolism. Aldolases from all species catalyze the reversible aldol cleavage of fructose 1,6-bisphosphate (Fru-1,6-P_2) into the triose phosphates, D-glyceraldehyde 3-phosphate and dihydroxyacetone phosphate. Catalysis proceeds by two distinct chemical pathways in aldolases. In class I aldolases, found in plants and higher animals, catalysis depends upon Schiff-base formation with the substrate (1), whereas in class II aldolases, found mostly in molds and bacteria, catalysis requires a metal cofactor such as Zn^{2+} (2). Demonstrable activity by aldolases also exists toward substrates such as fructose 1-phosphate (Fru-1-*P*), and the differential activity by aldolases toward Fru-1,6-P_2 and Fru-1-*P* has been used as a basis to discriminate between the various isozymes in vertebrates (3). In rabbit tissues, aldolase A has been isolated from muscle, aldolase B from liver, and aldolase C from brain. The three forms have been purified to homogeneity and extensively characterized (3–5). The enzymes have a relative molecular mass (M_r) of approximately 158,000 and a tertiary structure composed of four identical subunits spatially related by 222-fold symmetry (6, 7).

The catalytic cycle of the class I aldolase from rabbit skeletal muscle has been the most intensively studied and, on the basis of the experimental data, aldol cleavage proceeds through formation of a discrete number of enzyme–substrate intermediates (8–11). Rabbit skeletal muscle aldolase has been sequenced (12–15) and extensively covalently modified to determine essential amino acids participating in the catalytic cycle (1, 16–21). Although it has been possible to unequivocally establish the residues required for Schiff-base formation (1, 6) and C-6 phosphate binding to the enzyme (19–21), other active-site amino acid residues have either been assigned equivocally or have escaped identification entirely.

Aldolase A, which is present in large amounts in muscle tissue (22), has been crystallized in many different forms (23–28). Here we report that the catalytically active conformer of rabbit skeletal muscle aldolase (29) at 2.7-Å resolution corresponds to a singly wound β-barrel, and, on the basis of the determined structure and reported biochemical data, we delineate the residues composing the active site, which is located in the center of the aldolase β-barrel. The active-site residues have been conserved throughout evolution in all class I aldolases sequenced to date. Catalysis appears to be mediated by a mobile but highly nonhomologous COOH-terminal region, and it is proposed that the specific activities that aldolases exhibit toward their substrates may depend in part upon the amino acid sequence of the given COOH-terminal strand.

MATERIALS AND METHODS

Data Collection. Structural determination was carried out by using the monoclinic crystal form of rabbit skeletal muscle aldolase (space group $P2_1$, a = 164.0 Å, b = 57.5 Å, c = 85.1 Å, β = 102.7°, one tetramer per asymmetric unit). Data were collected on parent protein crystals to 2.7-Å resolution and from one suitable heavy-atom derivative, $Pt(CN)_4^{2-}$, to 2.9-Å resolution. Data collection method and solution of heavy-atom positions have been described (6) and are summarized in Table 1. During the course of data-merging, high solution intensities yielded systematically poorer statistics than did equivalent weak reflections measured at low resolution. Improvement in the merging statistics resulted when better models were used in the data-reduction step to correct for crystal x-ray radiation damage (data to be presented elsewhere) and mother-liquor absorption in the mounting capillaries. The new radiation damage correction included a dose-dependent transition state and allowed for anisotropic

The publication costs of this article were defrayed in part by page charge payment. This article must therefore be hereby marked "*advertisement*" in accordance with 18 U.S.C. §1734 solely to indicate this fact.

Abbreviations: Fru-1,6-P_2, fructose 1,6-bisphosphate; Fru-1-*P*, fructose 1-phosphate; SIR, single isomorphous replacement.

*To whom reprint requests should be addressed.

Table 1. Assessment of data quality

	Crystals used	Reflections measured	Unique reflections*	Merging R factors†	Goodness of fit‡
Native	35	96,796	42,333	0.048 (0.075)§	1.4
$Pt(CN)_4^{2-}$	24	58,952	—¶	0.015–0.039‖	1.1–2.5‖

*A reflection was rejected when its net intensity was less than zero. There were 450 and 45 such reflections in the native and $Pt(CN)_4^{2-}$ data sets, respectively.

†Merging R factors = $\Sigma_{h_i}|I_{h_i} - \langle I_h\rangle|/\langle I_h\rangle$, where I_{h_i} represents intensity of the ith observation of reflection h. Merging and scaling of the data was carried out by using the ROCKS crystallographic computing programs (30) and included all intensities >0.

‡Goodness of fit = $\Sigma_{h_i}\omega_{h_i}(I_{h_i} - \langle I_h\rangle)^2/(m-p)$, where $\omega_{h_i} = \sigma_{h_i}^{-2}$, m is the total number of overlapping reflections, and p is the number of scale factors. Variances $\sigma_{h_i}^2$ used were derived from counting statistics and various systematic corrections.

§In parentheses is the R factor for native data collected in the last shell at 2.7-Å resolution.

¶Intensity data for the heavy-atom refinement was divided into seven groups because it was found in the early stages of refinement that the native aldolase crystals exhibited variable reactivity toward the heavy-atom derivative (6). This variable reactivity could not be discerned by inspection of merging residuals because residuals between data sets on the basis of refinement having different $Pt(CN)_4^{2-}$ reactivities could be as low as 0.05. Data sets belonging to a group were chosen so that the overall goodness-of-fit was minimized within each group.

‖Minimum and maximum values for the statistic.

radiation damage in the crystal, thereby enabling recovery of intensity losses of up to 80% of the original intensity. Corrections for mother-liquor absorption in mounting capillaries, similar in functional form to corrections for crystal miscentering in the x-ray beam previously reported (7), modified the usual absorption corrections by as much as 40%. In each correction, the greatest impact was among the reflections at high resolution.

Phase Determination. Starting phase estimates for phase improvement by noncrystallographic symmetry averaging were obtained from SIR (single isomorphous replacement) refinement of the heavy-atom parameters; figure of merit and centric R factor were 0.40 and 0.52, respectively, for the final cycle of SIR refinement. Phases were refined in spheres of resolution to 2.9-Å resolution by real-space averaging of the interpreted electron densities of the four equivalent subunits (31) supplemented by solvent flattening. Heavy-atom positions were utilized to orient and position the 222-fold noncrystallographic rotation axes. The root-mean-square deviation of the heavy-atom positions from ideal 222 symmetry positions was <0.25 Å. Phase extension was carried out in shells of 0.05-Å resolution to phase reflections between 2.9- and 2.7-Å resolution. Convergence required a total of 22 cycles, which included first phase combination using phases derived from real-space averaging and SIR refinement to 2.9-Å resolution and then phase extension to 2.7-Å resolution. For 42,010 reflections phased, the final mean figure of merit was 0.72 and corresponded to an overall R factor (based on $|F|$) of 0.276.

Interpretation. Coordinates of the α carbons were obtained from a manual interpretation of a minimap using the known amino acid sequence (12–15). The measured C^α coordinates were then used to fit the appropriate amino acids to the electron density map of the aldolase subunit by using the computer program FRODO (32) implemented on an Evans–Sutherland color PS300, the results of which are shown schematically in Fig. 1. The computed electron density map was of sufficiently high quality to enable 329 of 363 amino acids to be unambiguously assigned within the electron density. Another 15 residues were located in regions of weak density on the surface of the tetramer, and portions of the last 18 amino acids of the COOH-terminal region are not sufficiently ordered for an unequivocal interpretation of the electron density of the COOH terminus.

RESULTS AND DISCUSSION

Subunit Structure. The polypeptide chain of the aldolase subunit folds into a single highly compact domain structure (Fig. 2) and is analogous to the singly wound parallel β-barrel motif (34) of the parallel α/β class structures. Among the various β-barrel proteins known (33, 35–41), aldolase displays the greatest structural similarity to the smaller yet functionally similar enzyme in bacteria, phosphogluconate aldolase (33). The bacterial enzyme, whose entire secondary structure organization matches that of the muscle isozyme, appears to be a more streamlined version of muscle aldolase. Because of its fewer amino acid residues, the structural simplification in the bacterial enzyme results in fewer helical turns in the flanking helices of the β-barrel and shorter loop regions connecting the β strands of the β-barrel to the flanking helices.

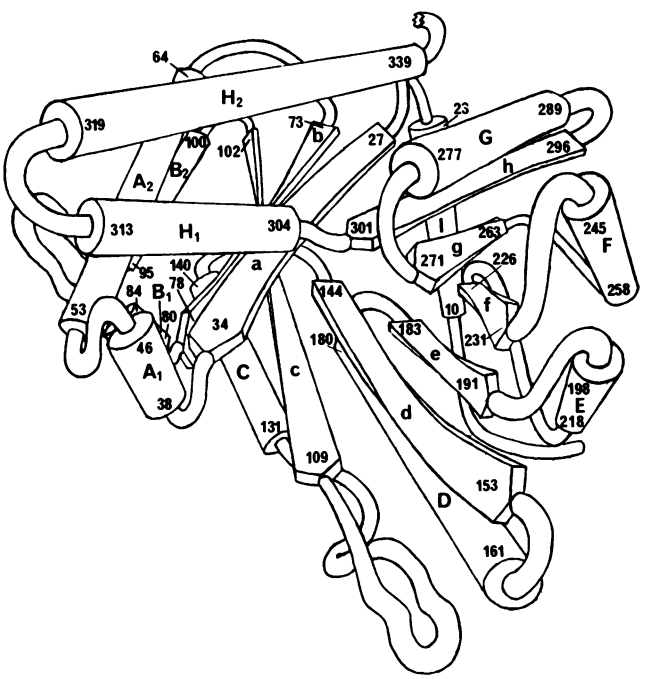

FIG. 1. Schematic drawing of the trace of the polypeptide in a subunit of rabbit skeletal muscle aldolase. Regions in β-sheet structure are represented by arrow-like bars (a–h), whereas those regions in α-helix are represented by tubes (A_1–H_2). The numbering indicates the first and last residue of the amino acid sequence corresponding to each region. Assignment of the lettering to the structural motifs is as in phosphogluconate aldolase (33). The symbol (+) corresponds to the intersection of the 222-fold molecular symmetry axes relative to the subunit and shows the orientation of two 2-fold rotation axes that are contained in the plane of the drawing.

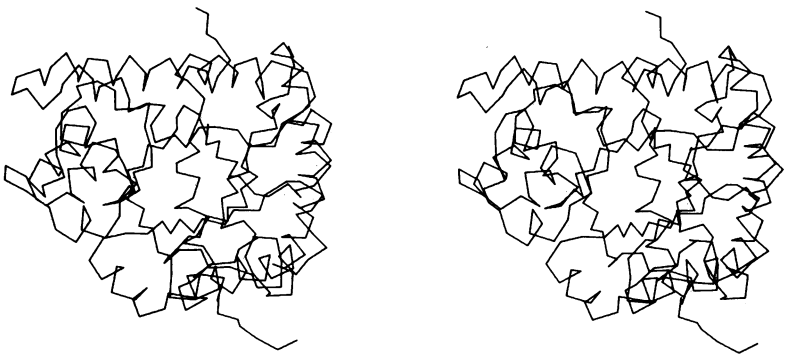

FIG. 2. Stereo drawing of the C^{α} backbone of a subunit of rabbit skeletal muscle aldolase. The orientation of the subunit has been chosen to maximize its resemblance with phosphogluconate aldolase (33).

The structure of the aldolase β-barrel, however, when compared with previous β-barrel structures whose amino acid sequence has been determined, is somewhat unusual in that the interior of the aldolase β-barrel is composed as expected not only of hydrophobic amino acid residues but also of potentially charged residues. According to our interpretation of the electron density map (Fig. 3), the residues Asp-33, Lys-107, Lys-146, Glu-187, and Lys-229 are all found in the interior cavity of the β-barrel. The charged moieties of these residues are approximately colinear with acidic and basic residues disposed in an alternating manner. This arrangement could afford neutralization of potential charges on these residues and, thus, permit the folding of these residues into the β-barrel interior.

Oxidation of transiently reactive enzyme carbanion intermediates in aldolase crosslinks Lys-229 [implicated in Schiff-base formation (1)] with Lys-146 (16). Affinity labeling of the active site with a competitive-inhibitor analogue of ATP has placed Lys-107 and Tyr-363 in close proximity (17), whereas labeling by alkylation preferentially alkylates residues His-361 and Lys-146 (18). In our structure the three lysine residues 107, 146, and 229 are located almost directly in line, spaced approximately 4 Å apart. Density is also found over the COOH edge of the β strands of the β-barrel in the vicinity of Lys-107 and Lys-146 and can be fitted by residues Ser^{355}-Leu^{356}-Phe^{357}-Ile^{358}-Ser^{359}. However, in view of the apparent disorder of the intervening residues 346–354 of the COOH terminus, unambiguous interpretation cannot yet be made as to the identity of this density. Our interpretation of the terminal peptide location places no definitive geometrical constraint on the alignment of the intervening residues on the subunit surface. Furthermore, the amino acid sequence of the intervening peptide is itself suggestive of considerable conformational flexibility, since it is rich in both glycines (residues 346 and 349) and alanines (residues 348, 350, 351, and 352)—residues that do not impose strong stereochemical constraints on the conformation of the intervening peptide.

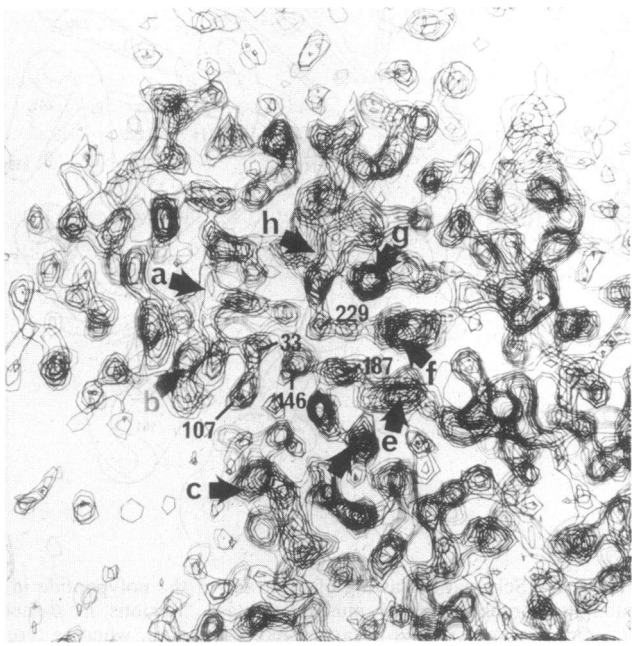

FIG. 3. A 6-Å-thick slice of electron density taken through the middle of the β strands e, f, and g of an aldolase subunit oriented as in Fig. 1. The β strands are indicated by thick arrows and are identified as in Fig. 1. Potentially charged residues in the center of the β-barrel are indicated and include Lys-107, Asp-33, Lys-146, Glu-187, and Lys-229.

Active Site. The amino acid residues implicated in the cleavage of Fru-1,6-P_2 are located in a pocket-like region that extends from the subunit surface to the center of the β-barrel and includes the region of potentially charged residues found in the center of the β-barrel described in Fig. 3. The location of the active site differs with respect to other β-barrel structures whose active-site residues have been determined.† In these β-barrel structures, the active-site regions have been found within the loop regions at the COOH edge of the β strands composing the β-barrel (42). In aldolase the lysine residue Lys-229, which is implicated in the Schiff-base formation with the C-2 carbon of the substrate, projects into the center of the β-barrel from the middle of β strand *f* (Fig. 4).

The known C-6 phosphate binding residue, Lys-107 (19–21), is at the surface of the binding pocket and can form an ion pair with Asp-33. However, the alignment of the COOH groups of Asp-33 and of Glu-187 further in the interior of the active site is such that they appear to mediate primarily potential repulsions between the ε-amino groups of adjacent lysine residues 107, 146, and 229 rather than to participate in ion-pair formation. The colinear alignment of the three lysine residues would be highly favorable for binding triphosphate moieties such as those in ATP (17) or inositol triphosphate (44), potent competitive inhibitors of aldolase. The interior

†An inhibitor-binding locus described in the low resolution structural study of rabbit muscle aldolase (6), when positioned on the 2.7-Å resolution map, corresponds to a region on the subunit surface devoid of electron density and triangulates to the vicinity of the NH_2 terminus of α-helix H_1, which is approximately equidistant between the last interpreted residue 345 and the density tentatively associated with residue 355. Although this location is some 12 Å from the active-site binding pocket, the low resolution electron density difference map suggests considerable conformational changes upon inhibitor binding throughout the subunit, including changes at the active-site locus. Definitive assignment of the inhibitor-binding locus and its relation to the native structure must consequently await analysis of high resolution studies on the liganded structure.

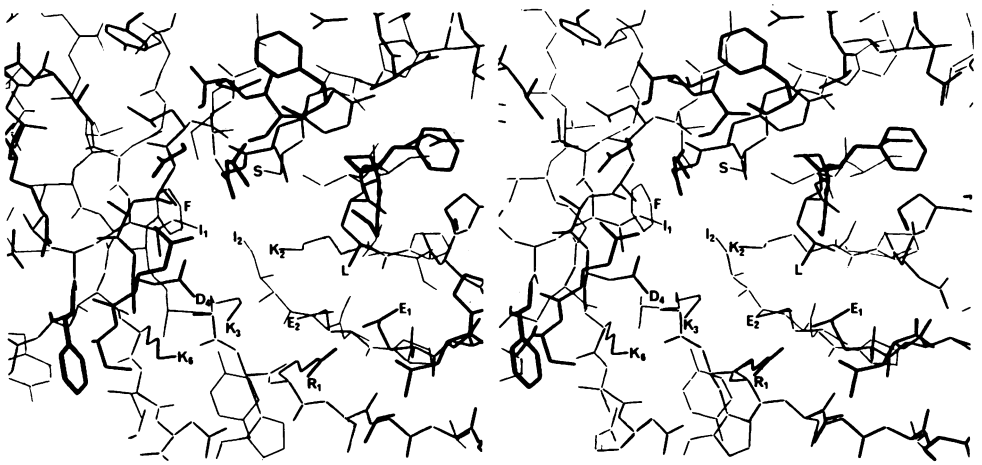

FIG. 4. Stereo drawing of the active-site residues of rabbit skeletal muscle aldolase. Active-site residues that have been completely conserved in all eukaryotic aldolases sequenced to date (43) are identified as follows: R_1, Arg-148; K_2, Lys-229; K_3, Lys-146; K_6, Lys-107; D_4, Asp-33; E_1, Glu-189; E_2, Glu-187; F, Phe-144; I_1, Ile-77; I_2, Ile-185; L, Leu-270; and S, Ser-300. The orientation of the subunit is the same as shown in Fig. 1 and corresponds to looking down into the center of the β-barrel from the COOH-edge side of the barrel β strands.

wall of the active-site pocket is lined by hydrophobic residues originating from all β strands. The hydrophobic residues nearest to the ε-amino group of Lys-229, Ile-185, Ile-77, and Phe-144 are located on the NH_2-terminal edge of the β-barrel and, together with α-helix I, block access to Lys-229 from the NH_2-terminal side of the β-barrel.

Arg-148, which has been considered a likely candidate for the C-1 phosphate binding site (18), is situated at the surface on the side opposite to Lys-107 of the binding pocket. The COOH group of Glu-189, which is in close proximity to the guanidine moiety of Arg-148, however, does not form an ion pair with Arg-148, but rather Arg-148 appears to bind a sulfate ion in our structure, consistent with a role by Arg-148 in phosphate binding. The distance between the two phosphate binding sites on the enzyme, 11 Å, compares favorably with C-1 phosphate-to-C-6 phosphate interatomic distances of Fru-1,6-P_2 in the acyclic configuration. However, binding by the α or β anomeric form of the substrate cannot be excluded because Arg-148 is not sterically hindered from adopting alternate conformations.

Influence of the COOH-Terminal Region on Catalytic Activity. Interpretation of the electron density map suggests that the polypeptide conformation of the COOH terminus, residues 341–363, corresponds to an arm-like structure possessing a highly flexible elbow joint (residues 346–354), which folds the polypeptide over the subunit surface from α-helix H_2 on the subunit exterior to the active site located in the β-barrel interior, the terminal amino acid residues of the folded COOH terminus being positioned so that they appear to cover the active site from the COOH edge of the β strands of the β-barrel. Preferential proteolysis of the COOH-terminal region (45–49) has been shown to diminish enzymatic activity to a basal level (46, 48), which is essentially independent of the length of the COOH terminus (48). It is then perhaps of significance that bacterial aldolase (33) appears to have lost the equivalent COOH-terminal region in its evolution. The apparent modulating role of the COOH-terminal peptide on catalytic activity suggests that the COOH-terminal peptide may function at the molecular level to promote, directly or indirectly, the alignment and/or attachment of the substrate during catalysis. Such a role implies conformational mobility by the COOH-terminal region to facilitate diffusion of substrate into and product out of the active site. The preferential proteolysis of the COOH-terminal region, which is abolished in the presence of substrate (45, 50), and the apparent disorder in the conformationally flexible region of the COOH-terminal peptide in the native structure are both consistent with such a postulated functional role.

Active Site Conservation. The alignment of the amino acid sequence of aldolases from human liver, rabbit muscle, maize, trypanosome, and *Drosophila* (43) strongly conserves the β-strand residues comprising the β-barrel. Comparison of the 63 amino acid residues making up the eight β strands shows only 7 residues of 20 nonhomologous residues to have undergone nonconservative substitution. All active-site amino acid residues, including the potentially charged groups in the interior of the β-barrel and the hydrophobic residues lining the active-site pocket, have been conserved throughout evolution of all class I aldolases. In contrast, only 4 residues of 22 residues in the COOH-terminal region have been conserved. The almost total lack of conservation of the

FIG. 5. Stereo drawing of the rabbit skeletal muscle aldolase tetramer. The tetrameric structure was generated from the 222-fold molecular symmetry applied to the subunit C^{α} backbone.

COOH-terminal region of the protein together with complete conservation of active-site residues suggests that the amino acid sequence in the COOH-terminal region of the protein may be implicated in determining the variable activity/specificity that aldolases exhibit toward their substrates.

Quaternary Structure. The spatial arrangement of the subunits in the aldolase tetramer is shown in Fig. 5. The subunit contacts are essentially all hydrophobic in nature, and the majority are between the flanking α-helices of the β-barrel, which are related by the two folds located in the plane of Fig. 5. Subunit close contacts arise principally from interactions between side chains of the symmetry-related flanking α-helices immediately connected to β strand *f*, which contains the active-site Lys-229. Contacts between subunits related by the noncrystallographic 2-fold axis perpendicular to this plane are fewer by comparison.

We thank L. Berthiaume for assistance in the art work and Dr. F. Quiocho and coworkers of Rice University for their generosity and assistance in the use of their graphics system and the National Research Council of Canada and the Fonds de Recherche en Santé du Québec for a scholarship to M.A. This work was funded by Medical Research Council of Canada Grant MT-8088.

1. Grazi, E., Cheng, T. & Horecker, B. L. (1962) *Biochem. Biophys. Res. Commun.* **7**, 250–253.
2. Rutter, W. J. (1964) *Fed. Proc. Fed. Am. Soc. Exp. Biol.* **23**, 1248–1257.
3. Penhoet, E., Kochman, M., Valentine, R. & Rutter, W. J. (1967) *Biochemistry* **6**, 2940–2949.
4. Penhoet, E., Rajkumer, T. & Rutter, W. J. (1966) *Proc. Natl. Acad. Sci. USA* **56**, 1275–1282.
5. Horecker, B. L., Tsolas, O. & Lai, C. Y. (1972) in *The Enzymes*, ed. Boyer, P. D. (Academic, New York), Vol. 7, pp. 213–258.
6. Sygusch, J., Boulet, H. & Beaudry, D. (1985) *J. Biol. Chem.* **260**, 15286–15290.
7. Sygusch, J. & Beaudry, D. (1985) *J. Mol. Biol.* **186**, 215–217.
8. Rose, I. A., O'Connell, E. L. & Mehler, A. H. (1965) *J. Biol. Chem.* **240**, 1758–1765.
9. Model, P., Ponticorvo, L. & Rittenberg, D. (1968) *Biochemistry* **7**, 1339–1347.
10. Healy, M. J. & Christen, P. (1973) *Biochemistry* **12**, 35–41.
11. Lai, C. Y., Tchola, O., Cheng, T. & Horecker, B. L. (1965) *J. Biol. Chem.* **240**, 1347–1350.
12. Lai, C. Y., Nakai, N. & Chang, D. (1974) *Science* **183**, 1204–1206.
13. Saygo, M. & Hajos, C. (1974) *Acta Biochim. Biophys. Acad. Sci. Hung.* **9**, 239–241.
14. Benfield, P. A., Forcina, B. G., Gibbons, I. & Perham, R. N. (1979) *Biochem. J.* **183**, 429–444.
15. Tolan, D. R., Amsden, A. B., Putney, S. D., Urdea, M. S. & Penhoet, E. E. (1984) *J. Biol. Chem.* **259**, 1127–1131.
16. Lubini, D. G. E. & Christen, P. (1979) *Proc. Natl. Acad. Sci. USA* **76**, 2527–2531.
17. Kasprzak, A. A. & Kochman, M. (1980) *Eur. J. Biochem.* **104**, 443–450.
18. Hartman, F. C. & Brown, J. P. (1976) *J. Biol. Chem.* **251**, 3057–3062.
19. Palczewski, K., Hargrave, P. A., Folta, E. J. & Kochman, M. (1985) *Eur. J. Biochem.* **146**, 309–314.
20. Shapiro, S., Enser, M., Pugh, E. & Horecker, B. L. (1968) *Arch. Biochem. Biophys.* **128**, 554–562.
21. Anai, M., Lai, C. Y. & Horecker, B. L. (1973) *Arch. Biochem. Biophys.* **156**, 712–719.
22. Penhoet, E. E., Kochman, M. & Rutter, W. J. (1969) *Biochemistry* **8**, 4396–4402.
23. Eagles, P. A. M., Johnson, L. N., Joynson, M. A., McMurray, C. H. & Gutfreund, H. (1969) *J. Mol. Biol.* **45**, 533–544.
24. Heidner, E. G., Weber, B. H. & Eisenberg, D. (1971) *Science* **171**, 677–680.
25. Miller, J. R., Shaw, P. J., Stammers, D. K. & Watson, W. C. (1981) *Philos. Trans. R. Soc. London. Ser.* **293**, 209–214.
26. Sawyer, L. 1(1972) *J. Mol. Biol.* **71**, 503–505.
27. Gorgunon, A. I., Andreyeva, N. S. & Spitsberg, V. L. (1969) *Biofizika* **14**, 1116–1117.
28. Brenner-Holzach, O. & Smith, J. D. G. (1982) *J. Biol. Chem.* **257**, 11747–11749.
29. Sygusch, J. & Beaudry, D. (1984) *J. Biol. Chem.* **259**, 10222–10227.
30. Reeke, G. N. R. (1984) *J. Appl. Crystallogr.* **17**, 125–130.
31. Bricogne, G. (1974) *Acta Crystallogr.* **A30**, 395–405.
32. Jones, A. T. (1978) *J. Appl. Crystallogr.* **11**, 268–272.
33. Lebioda, L., Hatada, M. H., Tulinsky, A. & Mavridis, I. M. (1982) *J. Mol. Biol.* **162**, 445–458.
34. Richardson, J. S. (1985) *Methods Enzymol.* **115**, 341–358.
35. Banner, D. W., Bloomer, A. C., Petsko, G. A., Phillips, D. C., Pogson, C. I., Wilson, I. A., Corran, P. H., Furth, A. J., Milman, J. D., Offord, R. E., Priddle, J. D. & Waley, S. G. (1975) *Nature (London)* **255**, 609–614.
36. Carrell, H. L., Rubin, B. H., Hurley, T. J. & Glusker, J. P. (1984) *J. Biol. Chem.* **259**, 3230–3236.
37. Stuart, D. I., Levine, M., Muirhead, H. & Stammers, D. K. (1979) *J. Mol. Biol.* **134**, 109–142.
38. Lindqvist, Y. & Brändén, C.-I. (1985) *Proc. Natl. Acad. Sci. USA* **82**, 6855–6859.
39. Schneider, G., Lindqvist, Y., Brändén, C.-I. & Lorimer, G. (1986) *EMBO J.* **5**, 3409–3415.
40. Xia, Z., Shamala, N., Bethge, P. H., Lim, L. W., Bellamy, H. D., Xuong, N. H., Lederer, F. & Mathews, F. S. (1987) *Proc. Natl. Acad. Sci. USA* **84**, 2629–2633.
41. Lins, L. W., Shamala, N., Mathews, F. S., McIntre, W., Singer, T. P. & Hopper, D. J. (1986) *Proc. Natl. Acad. Sci. USA* **83**, 4626–4630.
42. Brändén, C.-I. (1986) *Current Communications in Molecular Biology: Computer Graphics and Molecular Modelling* (Cold Spring Harbor Laboratory, Cold Spring Harbor, NY), pp. 45–51.
43. Kelly, P. M. & Tolan, D. R. (1987) *Plant Physiol.* **82**, 1076–1081.
44. Koppitz, B., Vogel, F. & Mayor, G. W. (1986) *Eur. J. Biochem.* **161**, 421–433.
45. Offermann, M. K., McKay, M. J., Marsh, M. W. & Bond, J. S. (1984) *J. Biol. Chem.* **259**, 8886–8891.
46. Humphreys, L., Reid, S. & Masters, C. (1986) *Int. J. Biochem.* **18**, 7–13.
47. Midelfort, C. F. & Mehler, A. H. (1972) *J. Biol. Chem.* **247**, 3618–3621.
48. Hannappel, E., MacGregor, J. S., Davoust, S. & Horecker, B. L. (1982) *Arch. Biochem. Biophys.* **214**, 293–298.
49. Bond, J. S. & Barrett, A. J. (1980) *Biochem. J.* **189**, 17–25.
50. Rose, I. A. & O'Connell, E. L. (1969) *J. Biol. Chem.* **244**, 126–134.